Anal. Bioanal. Electrochem., Vol. 17, No. 1, 2025, 1-17
https://www.doi.org/10.22034/abec.2025.720351

Analytical & Bioanalytical Electrochemistry

2025 by CEE
www.abechem.com

Full Paper

Potentials for Inhibiting Corrosion on Mild Steel using Various Borphosphate Glasses in 1 M HCl

Khadija Bougrine,[1] Issam Saber,[1] Hanane Barebita,[1] Soumya Ferraa,[1] Moussa Ouakki,[1,3,*] Mustapha Belfaquir,[2] and Mohamed Salahdine El youbi[1]

[1]*Laboratory of Organic Chemistry, Catalysis, and Environment, Faculty of Sciences, Ibn Tofaïl University, PO Box 133, Kenitra, 14000, Morocco*
[2]*Laboratory of Advanced Materials and Process Engineering, Faculty of Sciences, Ibn Tofail University, PO Box 133, Kénitra, 14000, Morocco*
[3]*National Higher School of Chemistry (NHSC), University Ibn Tofail BP. 133-14000, Kenitra, Morocco*

*Corresponding Author, Tel.: +212611749011
E-Mail: moussa.ouakki1@uit.ac.ma

Received: 8 September 2024 / Received in revised form: 4 January 2025 / Accepted: 17 January 2025 / Published online: 31 January 2025

Abstract- This study investigates the effectiveness of glassy compounds with the chemical formulation $30Li_2O$-$20ZnO$-xB_2O_3-$(50-x)P_2O_5$ as corrosion inhibitors for mild steel in a 1 M HCl solution. Using techniques such as polarization, impedance spectroscopy, and scanning electron microscopy (SEM), the anticorrosive properties of compounds P_1, P_2, and P_3 were evaluated. The results show that the inhibition efficiency increases with inhibitor concentration, reaching maximum values of 93.4%, 94.7%, and 96.3% for P_1, P_2, and P_3, respectively. Polarization analysis revealed that these compounds act as mixed inhibitors in hydrochloric acid. The SEM analysis indicated that the inhibitors adsorb onto the steel surface, reducing the corrosion effects. Compound P_3 exhibited the highest performance, with an inhibition efficiency of 96.3%, owing to its specific chemical structure that provides superior efficacy. These findings suggest that these glassy compounds have significant potential for specific industrial applications, emphasizing the importance of composition and concentration in optimizing their anticorrosive properties.

Keywords- Glassy substance; Polarization; Stoichiometry; Electrochemical methods; HCl; Corrosion inhibition

1. INTRODUCTION

Corrosion arises from the chemical and electrical interactions between metals, alloys, and their environment. It impacts various industries, including oil, chemicals, electricity, nuclear sectors, port facilities, as well as fields like civil engineering, healthcare, environmental management, and food processing. The consequences are particularly severe in the industrial sector, where production shutdowns, replacement of corroded components, accidents, and environmental hazards are common, often leading to significant financial losses. To address these challenges, techniques such as cathodic protection, surface treatments with metallic or polymer coatings, and the introduction of corrosion inhibitors to alter the corrosive environment are widely applied [1]. This is a novel approach to preventing rusting. When these substances are put in small amounts to corrosive conditions, they reduce or even eliminate the metal's reactivity with its environment. Putting two or more of these together protective measures is the current trend [2]. Researchers have been studying organic molecules as corrosion inhibitors for decades [3,7]. Rust inhibitors obstruct the crucial phase of the corrosion cycle known as the cathodic reduction process. After adsorption, the structure of the electrical double layer on the metal surface is modified. Metals are pivotal in energy generation processes. Several industrial inhibitors, particularly inorganic compounds like boric acid [8], permanganate [9], molybdate [10], phosphate [11,12], and glasses [13,14], have shown significant effectiveness.

There has been limited research on the use of borate-based glasses as corrosion inhibitors for mild steel. Adsorption may be promoted by functional groups and electronegative atoms. Various factors, including the type of metal and the environmental conditions, influence this process, have been examined in the comprehensive research on the properties of metal surfaces that hinder corrosion [15,16]. The inhibitor's molecular and electrical structures, as well as its solubility, are all covered in this thorough method. The efficiency of the inhibitor is influenced by variables like temperature, pH, and inhibitor concentration. The effectiveness of the inhibitor is largely dependent on its molecular structure. A thorough evaluation of its inhibitory performance is essential for understanding the practical application of these compounds.

In order to shield a 1.0 M HCl solution containing mild steel, this work proposes three inorganic corrosion inhibitors (borophosphate glass phases). Each of these molecules has a unique chemical structure. Each of these molecules has a unique chemical structure. Evaluation techniques for them include potentiodynamic studies, electrochemical impedance spectroscopy analysis, and surface characterization of mild steel with special attention to lithium glass, zinc, boron, and phosphate content.

This study presents a novel approach by investigating the use of borophosphate glasses as inhibitors for mild steel corrosion. While these materials have not been extensively explored for this application, the research highlights their promising potential to protect steel in acidic

environments. This opens up new possibilities for industrial applications and provides deeper insights into the mechanisms behind corrosion inhibition.

2. EXPERIMENTAL SECTION

2.1. Glass synthesis using borate

Samples of glass were created using the melt tempering technique. Precisely calculated amounts of high-purity (99.9%) diammonium hydrogen phosphate $(NH_4)_2HPO_4$ and boric acid H_3BO_3, zinc oxide ZnO, and lithium carbonate Li_2CO_3, all produced by stoichiometric mixing of raw components in accordance with the reaction (1):

$$\mathbf{0.3Li_2CO_3 + 0.2ZnO + 2x\,(H_3BO_3) + 2(0.5\text{-}x)\,(NH_4)_2\,HPO_4}$$

$$\downarrow$$

$$\mathbf{0.3Li_2O + 0.2ZnO + xB_2O_3 + (0.5\text{-}x)P_2O_5 + 0.35CO_2\uparrow + 1.5H_2O\uparrow + 2NH_3\uparrow}$$

For every particular composition, the samples were weighed and combined in a mortar. In platinum crucibles, the mixtures were heated to 200°C for four hours, and then to 350°C for twenty-four hours to remove volatile substances such CO_2, NH_3, and H_2O. After that, each reaction mixture was melted in a 1050°C oven, forcefully poured into a 200°C-preheated aluminum mold, and kept dry in desiccators to prevent moisture buildup. Table S1 contains a list of the compositions examined.

2.2. Measurements connected to electrochemistry

Table S2 lists the mild steel's chemical makeup that served as the study's substrate. The mild steel samples are carefully prepared before immersion. They are heat-dried using hot air, cleaned with distilled water, and polished with 1200-grit sandpaper. A 1 M hydrochloric acid solution, prepared from concentrated acid and distilled water, serves as the corrosive medium. All experiments were conducted at ambient temperature (298 K).

For electrochemical measurements, a three-electrode system was employed: a platinum electrode as the counter electrode, a saturated calomel electrode (SCE) as the reference, and mild steel as the working electrode. The working electrode had a surface area of 1 cm^2 in contact with the corrosive solution. Steady-state measurements were performed in potentiodynamic mode using a PGZ 100 potentiostat/galvanostat. Continuous open-circuit potential (OCP) was applied to mild steel specimens during their execution. At a scan rate of one millivolt per second, the sample's applied potential was continually altered. These curves were measured between -900 and -100 mV/SCE in the voltage range.

To find the corrosion current density (i_{corr}), as a function of the corrosion potential, the anodic and cathodic curves' linear Tafel slopes are extrapolated. The following formula (Eqn. 1) is used to determine the inhibitory efficacy [17]:

$$IE\ \%= [(i°_{corr} - i_{corr}) / i_{corr}] \times 100 \quad (1)$$

The corrosion current densities, both in the absence and presence of an inhibitor, are represented by the symbols $i°_{corr}$ and i_{corr}, respectively.

Similar to polarization curve analysis, electrochemical impedance measurements are performed within a frequency range of 100 kHz to 100 MHz, using a sinusoidal perturbation potential of 10 mV. The electrochemical impedance across this frequency range is determined from the corresponding plots, which provide valuable insights into the processes associated with the protective performance of inhibitors or coatings. The inhibitory efficiency is evaluated using Equation (Eqn. 2) [18]:

$$IE\ \% = [1 - (R^{o}_{ct} / R_{ct})] \times 100 \quad (2)$$

The charge transfer resistance in the presence and absence of an inhibitor is denoted by Rct and Roct, respectively.

2.3. Examination of the surface

The examined compounds, P_1, P_2, and P_3, were present or missing when the aluminum surface was submerged for six hours at 298 K in a solution containing 1.0 M of hydrochloric acid (HCl). This examination was carried out with the aid of an electronic balance microscope (MEB). Additionally, comprehensive elemental research was conducted by integrating an energy dispersive analysis (EDX) with the SEM apparatus.

3. RESULTS AND DISCUSSION

3.1. Impedance spectroscopy using electrochemistry

In this study, the inhibition of mild steel corrosion in a 1.0 M HCl solution is examined using electrochemical impedance spectroscopy.

The conditions with and without the application of inhibitors have been compared. Figure 1 illustrates the Nyquist plots, which characterize the behavior of mild steel under these different conditions and with varying concentrations of P_1, P_2, and P_3.

The presence of a single semicircle in each Nyquist plot indicates that charge transfer plays a predominant role in controlling the corrosion and protection mechanisms of mild steel [19-21]. However, the Nyquist diagrams exhibit compressed semicircle loops, deviating from an ideal semicircle. This behavior can be attributed to variations in the frequency dispersion of the interfacial impedance and the heterogeneous distribution of adsorbed species on the mild steel surface [22-24]. It is noteworthy that the topological structure of the Nyquist plots

remained consistent, indicating that the addition of inhibitors primarily increased the impedance value without significantly altering other electrochemical properties of the system.

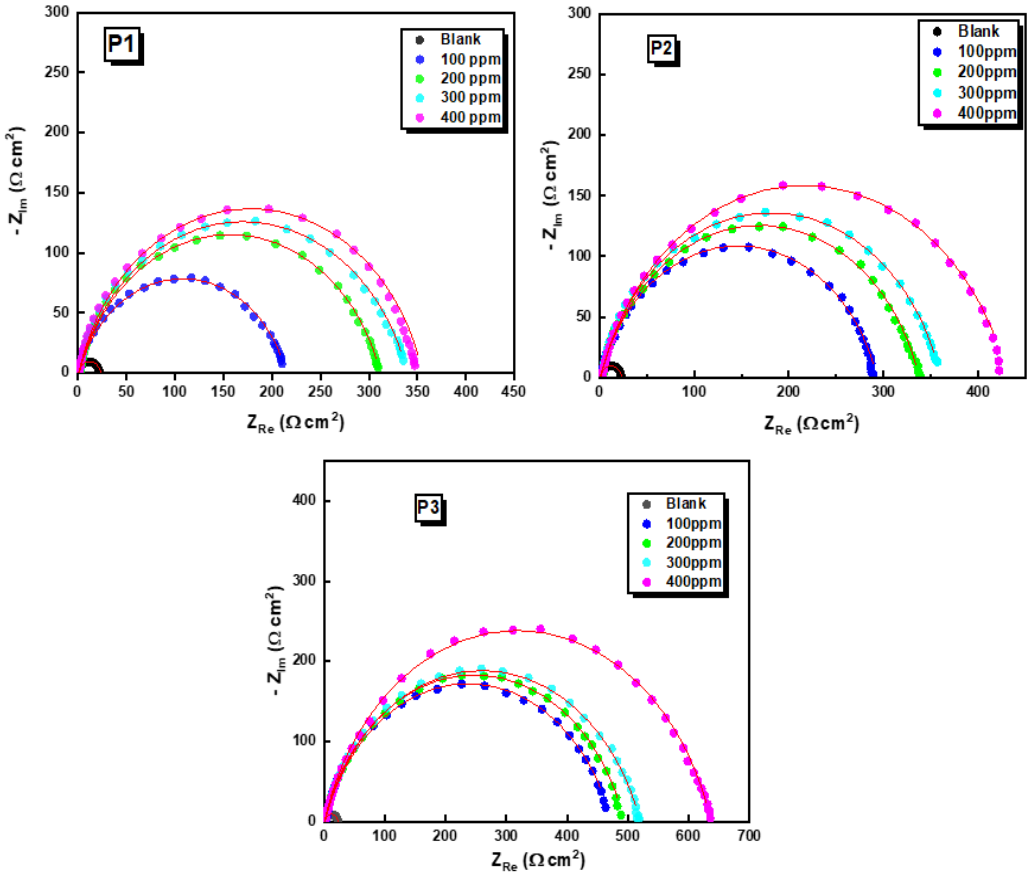

Figure 1. Graphs showing the impedance of mild steel in 1 M HCl for various inhibitor concentrations

As shown in Figure 2, analysis of the Bode diagram indicates the presence of a single peak in both the inhibited and uninhibited solutions. This observation serves to validate the analogous circuit model employed in the impedance spectrum calculations. Furthermore, the Bode diagrams illustrate that each inhibitor exhibits a single maximum phase angle, underscoring the conclusion that the primary determining factor of electrochemical interactions at the metal-solution interface is the rate of charge transfer [25].

The EIS data obtained was modeled using a similar circuit. Figure S1 shows the equivalent circuit which includes a solution resistor (R_s), a charge transfer resistor (R_{ct}), and a constant phase element (CPE) [26,27]. For this work, the effective double-layer capacitance (C_{dl}) values were calculated using the equation below (Eqn.3).

$$C_{dl} = \left[QR_{ct}{}^{1-n}\right]^{1/n} \qquad (3)$$

Table 1 displays all of the electrochemical parameters that were determined by altering the Nyquist diagrams. The compounds' corrosion inhibition efficiency (η) can be determined by applying the subsequent formula (Eqn.4) [18].

$$\eta_{EIS}(\%) = \frac{R_{ct} - R_{ct}^{\circ}}{R_{ct}} \times 100 \qquad (4)$$

Where R_{ct} is the resistance to polarisation with an inhibitor and R_{ct}° is the resistance to polarisation without an inhibitor.

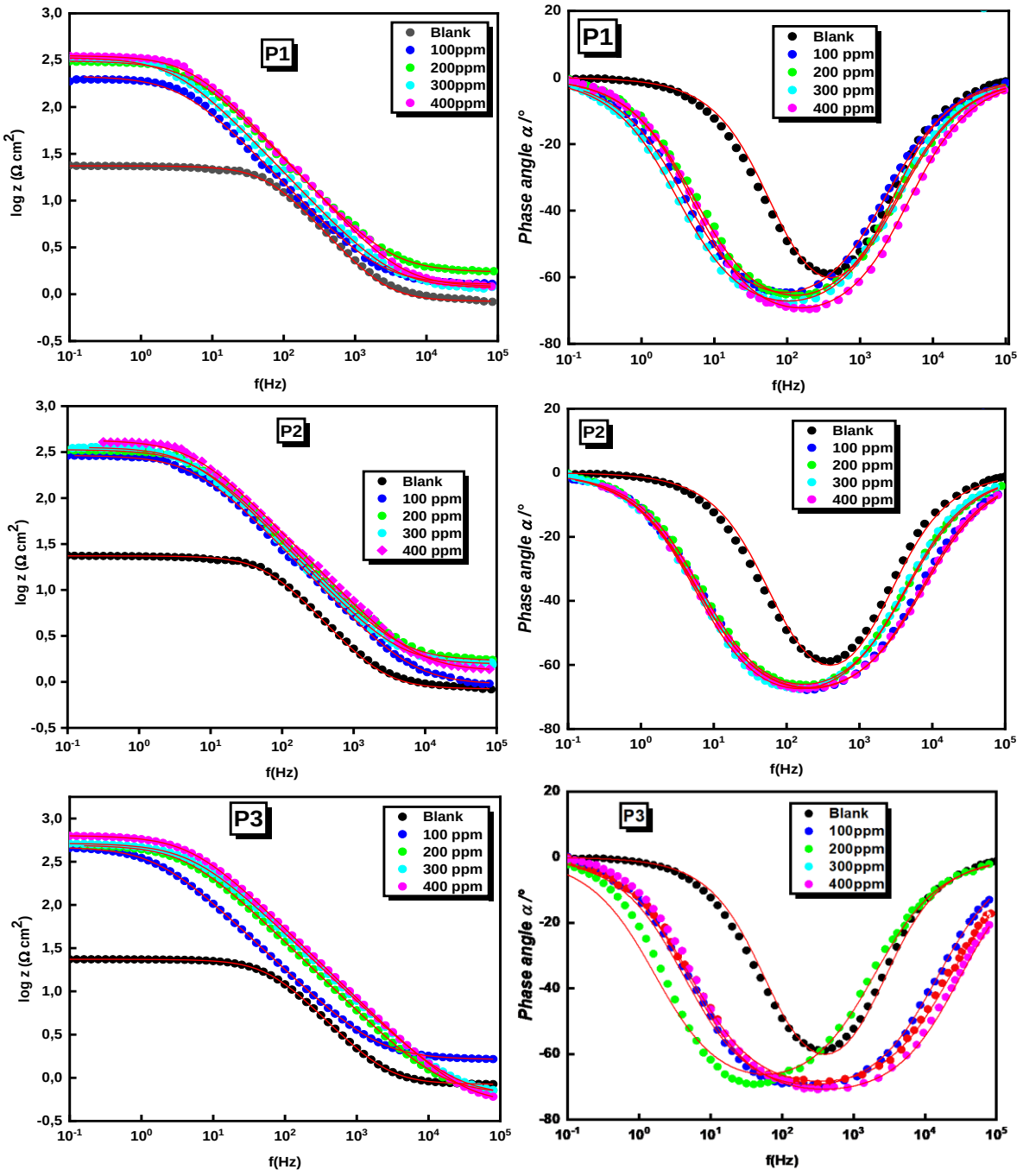

Figure 2. The Bode diagrams show mild steel in molar HCl (white) and with varying inhibitor concentrations

Table 1. The EIS study's electrochemical results on mild steel corrosion in both inhibited and non-inhibited solutions at 298 K

Medium	**Conc (ppm)**	**R_s ($\Omega.cm^2$)**	**Q ($\mu F.S^{n-1}$)**	**n**	**C_{dl} ($\mu F\ cm^{-2}$)**	**R_{ct} ($\Omega.cm^2$)**	**η_{imp} %**
Blank	--	0.8	211	0.9	114.0	22.7	-
P1	100	1.2	355	0.8	192.9	213.4	89.1
	200	1.7	184	0.8	96.5	309.8	92.6
	300	1.1	258	0.8	149.2	338.1	93.2
	400	1.1	153	0.8	87.6	353.8	**93.5**
P2	100	0.9	175	0.8	89.7	291.9	92.2
	200	1.6	138	0.8	70.0	335.8	93.2
	300	1.5	144	0.8	77.9	358.5	94.4
	400	1.3	125	0.8	63.5	429.5	**94.7**
P3	100	1.6	319	0.8	201	471.0	95.1
	200	0.6	138	0.8	75.2	493.4	95.3
	300	0.6	120	0.8	60.2	519.5	95.6
	400	0.5	93	0.8	50.3	636.3	**96.3**

As the inhibitor concentration increases, the double-layer capacitance (C_{dl}), Q coefficient, and charge transfer resistance (R_{ct}) all decrease, which enhances the corrosion resistance of mild steel. This behavior indicates that the inhibitors are adsorbed onto the electrode surface, thereby improving the inhibition efficiency in the aggressive environment studied, with P3 achieving an inhibition efficiency of 96.3%. This result highlights the crucial role of the compositional characteristics of the treated glass in its ability to inhibit corrosion.

3.2. Potentiodynamic polarization

3.2.1. Influence of concentration

The corrosion behavior of mild steel in an acidic environment was evaluated using potentiodynamic polarization measurements (Figure 3). The results demonstrate that the inhibitors P1, P2, and P3, when added to a 1.0 M HCl solution, influence both anodic and cathodic reactions. This effect is attributed to the adsorption of the inhibitors onto the metal surface, which reduces metal dissolution and slows down the hydrogen ion reduction. Additionally, the parallel alignment of the cathodic curves indicates that the inhibitors have a minimal impact on the hydrogen ion reduction process, confirming that charge transfer remains the predominant mechanism for hydrogen release.

The electrochemical parameters, including the corrosion current density (i_{corr}), corrosion potential (E_{corr}), cathodic and anodic Tafel slopes (β_c, β_a), as well as the calculated inhibitory efficiencies, are summarized in Table 2.

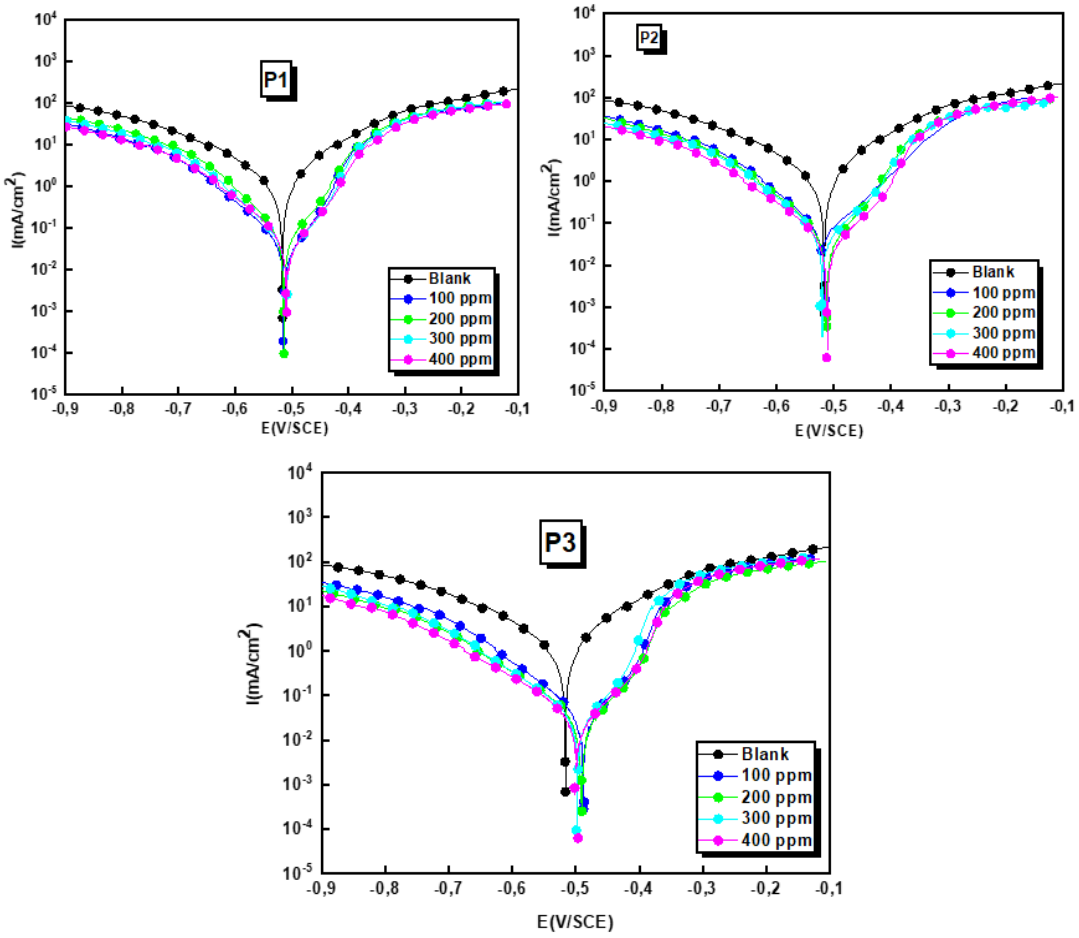

Figure 3. Polarisation curves for mild steel in 1 M HCl in the absence and presence of various inhibitor concentrations and at various temperatures

Table 2. At 298 K, the potentiodynamic polarization of mild steel in 1.0 M HCl was examined both with and without varying inhibitor doses

Medium	Conc. (ppm)	- E_{corr} mV/SCE	i_{corr} µA cm^{-2}	$-\beta_c$ mV dec^{-1}	β_a mV dec^{-1}	η_{PP} %
Blank	--	**515**	**1 045**	**133**	**134**	--
P1	100	510	118.0	125	131	88.7
	200	513	87.7	131	128	91.6
	300	506	75.2	124	123	92.8
	400	507	68.9	122	126	**93.4**
P2	100	513	91.9	119	130	91.2
	200	510	74.1	123	123	92.9
	300	510	64.7	126	126	93.8
	400	517	55.3	128	121	**94.7**
P3	100	492	61.6	118	129	94.1
	200	490	55.3	127	132	94.7
	300	495	48.0	130	125	95.4
	400	485	39.7	131	127	**96.2**

Analysis of Table 2 shows that the anodic (β_a) and cathodic (β_c) slopes fluctuate as a function of their concentrations, indicating alterations to the iron dissolving process and oxygen reduction, respectively. These findings demonstrate a reduction in the corrosion current density, leading to a notably high inhibitory efficiency (E%) in the presence of these compounds at a concentration of 400 ppm. A significant increase in cathodic current densities is observed at this concentration. Furthermore, the addition of inhibitors in 1 M HCl results in a shift of the corrosion potential toward more negative values. The inhibitory efficiency improves with increasing inhibitor concentration, reaching a peak of 96.2% at 400 ppm for P3. The glasses studied show a difference in efficiency due to the presence of B_2O_3.

3.2.2. Influence of temperature

The effect of temperature on the efficacy of inhibitors has been the subject of extensive research, particularly in the context of acidic environments. Potentiodynamic tests were conducted at varying temperatures to evaluate the impact of temperature on the inhibitory efficiency of materials synthesized in a 1.0 M HCl solution. Figure 4 presents the potentiodynamic polarization curves for mild steel in 1.0 M HCl, both with and without the presence of inhibitors.

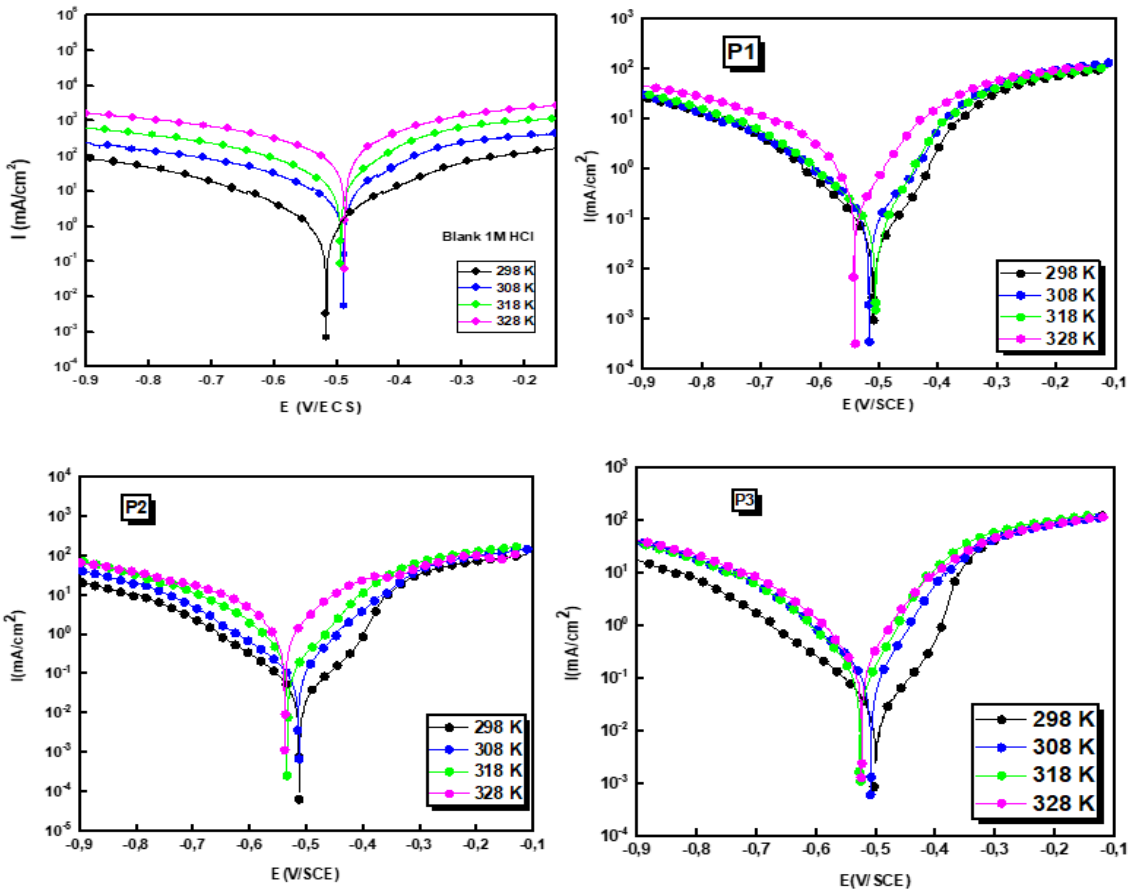

Figure 4. Polarisation curves for mild steel in 1 M HCl were obtained in the absence and presence of various inhibitor concentrations and at various temperatures

The Tafel plots provide unambiguous depictions of the anodic and cathodic branches, with the former increasing in length as the temperature rises. The cathodic branch exhibits a parallel trend, suggesting a unidirectional activation process that functions across the entire temperature range, leading to the reduction of H^+ ions on the steel surface. Concurrently, the corrosion potential, E_{corr}, approaches maximum values at each temperature. Table S3 provides a comprehensive overview of the inhibition efficiency (E%) and electrochemical characteristics associated with steel corrosion in 1 M HCl, both prior to and following the addition and testing of inhibitors at multiple temperatures.

The data presented in Table S3 clearly indicate that current densities rise with an increase in temperature. Generally, higher temperatures can promote the desorption of absorbed inhibitors and accelerate the dissolution of the metal [28]. As shown in the results, the inhibitory efficiency decreases slightly with increasing temperature. Based on these findings, we suggest that these compounds are most effective in preventing corrosion of mild steel in 1 M HCl at a temperature of 298 ±2 K.

To better understand the nature of the inhibitor adsorption, the variations in the logarithm of the corrosion current density as a function of the reciprocal temperature (1000/T) were examined and presented in Figures S2 and S3.

The change in ln (i_{corr}) = f (1000 / T) is linear. The slope of the resulting lines is utilized to determine the activation energies (Ea) based on the Arrhenius expression (Eqn.5) [29].

$$i_{corr} = A_{exp}\ ((-E_a) / RT) \qquad (5)$$

T is the absolute temperature (K), A is the pre-exposure factor, R is the ideal gas constant, and i_{corr} is the corrosion current density. Equation (Eqn.6) provides an alternative variant of the Arrhenius equation that can be used to compute activation enthalpy (H_a) and activation entropy (S_a) values [30].

$$i_{corr} = \frac{RT}{Nh} exp\left(\frac{\Delta S_a}{R}\right) exp\left(-\frac{\Delta H_a}{RT}\right) \qquad (6)$$

Where h is Planck's constant and N is Avogadro's number. Figure S3 shows the evolution of ln(icorr/T) as a function of the inverse of temperature in the form of a straight line with slope (-ΔHa/R) [31]. By extrapolating these lines, we obtain the values of (Ln (R/Nh) + S_a/R), i.e [32], those of ΔH_a and ΔS_a. The results obtained are shown in Table 3.

As shown in Table 3, the solutions containing P1, P2, and P3 exhibit higher activation energies compared to the uninhibited solution. This can be attributed to the formation of a protective layer on the mild steel surface, which reduces corrosion. The positive ΔH_a highlights the endothermic nature of the mild steel dissolution process [33,34]. Furthermore, the higher ΔS_a observed in the presence of inhibitors suggests a decrease in system disorder due to the formation of metal complexes or adsorbed species [35-38]. Finally, the thermodynamic parameters ΔH_a and ΔS_a were determined by plotting (i_{corr}/T) as a function of the inverse of temperature (1000/T). The significant positive values of ΔH_a and negative values of ΔS_a in the

presence of inhibitors indicate that these substances effectively slow down the dissolution of mild steel in the given environment.

Table 3. Analysis of the activation parameters for the dissolution of mild steel in 1.0 M HCl, both with and without inhibitors

Medium	**E_a (Kj/mol)**	**ΔH_a (Kj/mol)**	**ΔS_a (J/mol.K)**
Blank	28.7	26.2	-99.2
P_1	43.3	40.73	-73.39
P_2	40.9	38.35	-82.68
P_3	45.6	43.00	-69.52

3.3. Adsorption isotherm

Metal corrosion can result in two different forms of interaction with the metal surface: physisorption and chemisorption. The adsorption of organic or inorganic molecules onto the metal surface slows metal corrosion. The factors influencing the adsorption process include loading, metal surface characteristics, inhibitor chemical structure, and electrolyte type [38]. The characterization of the adsorption process frequently involves the employment of various adsorption isotherms, including Temkin, Frumkin, Langmuir, and Flory-Huggins [39–42]. The Langmuir adsorption isotherm is widely regarded as the most appropriate model for this purpose. The following circumstances illustrate the manner in which the surface of mild steel absorbs inhibitor compounds when the Langmuir adsorption isotherm is utilized [43]. The Langmuir isotherm model demonstrates a direct correlation between C/θ and C, despite the fact that the slopes for all the chemicals tested are never greater than unity. Predictions based on Langmuir's theories about the absence of intermolecular interactions and the homogeneity of adsorption sites should ideally respect a value of 1 for the slope. Figure S4 shows straight lines with a linear association ($R^2 \simeq 1.00$ for our inhibitors) following the application of the Langmuir model extrapolation approach (Eqn. 7). This finding suggests that the observed relationship corresponds to the Langmuir adsorption isotherm, a model that our inhibitors appear to adhere to during the process of adsorption in an acidic solution onto a metal surface [44].

$$\frac{Cinh}{\theta} = \frac{1}{Kads} + Cinh \qquad (7)$$

Where K_{ads} represents the adsorption constant, θ represents the surface coverage and C represents the concentration of the antagonist. According to the literature, the adsorption equilibrium constant (K_{ads}) correlates well with the standard free energy of adsorption (ΔG_{ads}) according to the following relationship (Eqn. 8) [45]:

$$\Delta G_{ads} = -\,RT \ln (1000\, K_{ads}) \qquad (8)$$

Where R represents the universal gas constant, T the absolute temperature and 1000 the water concentration in the formula. The ΔG_{ads} are determined and grouped in Table 4. The negative values of the free energy of adsorption ΔG_{ads} suggest spontaneous adsorption of the glassy compounds onto the metal surface and intense interaction between the inhibitor molecules and the mild steel surface [46,47].

Table 4. Assessment of the constant K and adsorption energy ΔG_{ads} values

Inhibitors	**K_{ads} (L/g)**	**ΔG_{ads} (Kj/mol)**	**R^2**
P_1	15.8202	-23.9	0.99999
P_2	21.9154	-24.7	0.99999
P_3	41.6840	-26.3	0.99998

It is generally accepted that values of ΔG_{ads} close to -20 kJ/mol or lower indicate electrostatic interactions between charged molecules and a charged metal surface (physical adsorption), while values close to -40 kJ/mol or lower suggest charge sharing or transfer of inhibitor molecules to the metal surface, forming a coordinated covalent bond (chemical adsorption) [48-50]. In the present case, the free enthalpy of adsorption is approximately -20 kJ/mol, suggesting that the inhibitors are adsorbed onto the steel surface through physisorption.

3.4. Surface analysis

In addition to quantitative EDX investigations, qualitative SEM microscopic analyses were conducted to confirm the electrochemical testing results (Figure 5).

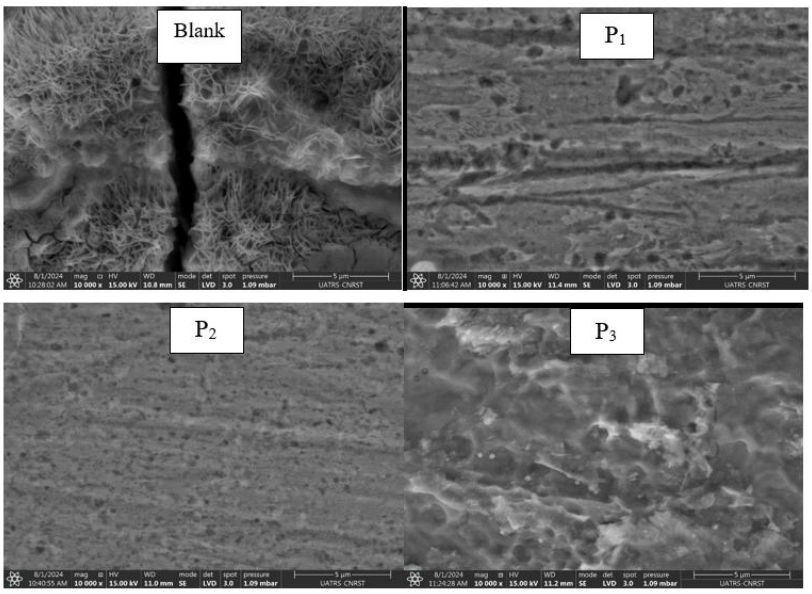

Figure 5. SEM of mild steel in 1 M HCl at room temperature, without and with different concentrations of inhibitors

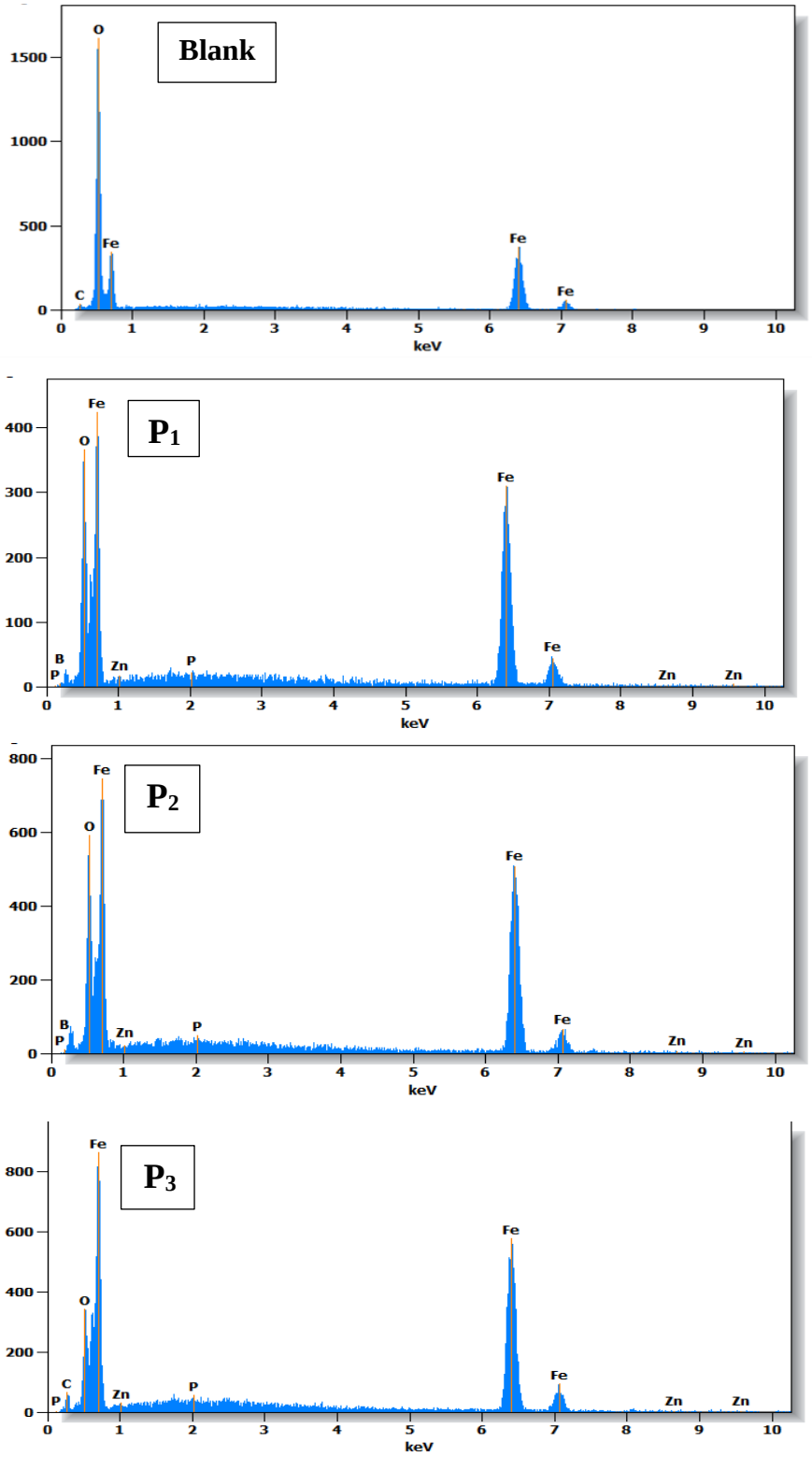

Figure 6. Qualitative and quantitative analysis of mild steel using EDX, following 6 hours of immersion

SEM images of the mild steel surface were taken after 6 h of immersion in 1.0 M HCl at 298 K, both before and after the addition of P1, P2, and P3. The image clearly shows signs of

corrosion on the steel surface after 6 hours of exposure to 1.0 M HCl at 298 K in the absence of the inhibitor. However, when the glassy compounds P1, P2, and P3 were added, the SEM micrographs of the steel surface, after 6 hours of immersion in the same solution containing 100 ppm of the inhibitors, revealed a wafer-shaped product covering the surface, indicating adsorption of the glassy phase [51]. This observation suggests that the inhibition mechanism involves the formation of a stable, insoluble adhesive layer that limits the access of the electrolyte to the steel surface. The EDX spectrum shown in Figure 6 confirms the formation of iron oxide and the presence of an oxygen peak in the blank, following the etching of the steel in 1.0 M HCl.

In both a blank solution of 1.0 M HCl and the solution containing the inhibitors P_1, P_2, and P_3, the peaks corresponding to carbon and oxygen were notably reduced in the samples treated with the glassy inhibitors P_1, P_2, and P_3. The glassy compounds' ability to suppress mild steel's electrolytic corrosion of the substrate is validated by the spectroscopic data, indicating their significance in the development of a protective layer. In conclusion, the experimental results validate glassy compounds' efficacy against mild steel corrosion. By preventing the electrolyte from reaching the steel surface, these chemicals form a sticky and insoluble coating that accelerates the metal's corrosive degradation in acidic environments.

4. CONCLUSION

Based on the detailed analysis provided in this study, which investigates the corrosion inhibition of mild steel in acidic environments using synthetic glassy compounds with the chemical composition $30Li_2O\text{-}20ZnO\text{-}xB_2O_3\text{-}(50\text{-}x)P_2O_5$, it can be concluded that these glassy compounds exhibit substantial inhibitory effects on the corrosion of mild steel. The experimental results indicate that the addition of these glassy inhibitors significantly reduces the corrosion current density in the acid solution and enhances polarization resistance. The reduction of corrosion is directly impacted by the glass phases compositional characteristics. More specifically, at 400 ppm, the compound P3 exhibits a 96.2 percent performance inhibitor as compared to other samples. These outcomes validate his goal. Increasing the concentration of component x leads to enhanced inhibition. It is crucial to consider how sensitive these inhibitors are to heat. From the results, it can be inferred that temperature affects a chemical product's ability to inhibit growth. It is important to exercise caution when using these inhibitors in high temperature environmental conditions due to this effect, which highlights their thermal sensitivity. They lessen the cathodic reactions necessary for the corrosion process by functioning as cathodic inhibitors. It is important to note that P_3 demonstrates greater effectiveness in inhibiting corrosion at elevated temperatures compared to P_1 and P_2. A comprehensive examination of corrosion kinetics in relation to temperature has facilitated our comprehension of the inhibitor mechanism. Glassy chemicals physically adsorb on the steel's surface, occulting the active sites and counteracting the effects of corrosion. It is feasible to

clarify how these glassy substances effectively prevent rusting and investigate potential advancements for particular industrial applications by comprehending their mode of action.

Declarations of interest

The authors declare no conflict of interest in this reported work.

REFERENCES

[1] G. Beranger, and M. Henri, Corrosion and anticorrosion. Industrial practice. Edition Technique Documentation, Lavoisier, Paris 303 (2002).

[2] I. Bouali, Study of metal corrosion inhibitors based on functionalized lamellar zirconium orthophosphates: synthesis, characterizations and applications. Diss. University of Lorraine; Cadi Ayyad University, Marrakech, Morocco (2018).

[3] M. Lgaz, H. Dassanayake, R. Salghi. R. Jodeh, S. Abidi, N. Hamed, and O. Guar, J. Mol. Structure 1145 (2017) 43.

[4] C. Verma, L.O. Olasunkanmi, I.B. Lgaz, M.A. Quraishi, J. Haque, E.S. Sherif, and E.E. Ebenso, J. Mol. Liq. 273 (2019) 1.

[5] S. Sengupta, M. Murmu, N.C. Murmu, and P. Banerjee, J. Mol. Liq. 326 (2021) 115215.

[6] D.B. Tripathy, M. Murmu, P. Banerjee, and M.A. Quraishi, Desalination 472 (2019) 114128.

[7] A. Singh, K.R. Ansari, M.A. Quraishi, S. Kaya, and P. Banerjee, New J. Chem. 4316 (2019) 6303.

[8] M.E. Mashuga, L.O. Olasunkanmi, A.S. Adekunle, S. Yesudass, M.M. Kabanda, and E.E. Ebenso, Materials 8 (2015) 3607.

[9] V.S. Sastri, Corrosion Inhibitors: Principles and Applications, John Wiley & Sons: New York, USA (1998).

[10] J.N. Asegbeloyin, P.M. Ejikeme, L.O. Olasunkanmi, A.S. Adekunle, and E.E. Ebenso, Materials 8 (2015) 2918.

[11] A. Elbadaoui, M. Galai, S. Ferraa, H. Barebita, M. Cherkaoui, and T. Guedira, Mediterranean J. Chem. 8 (2019) 328.

[12] M. Bouklah, O. Krim, M. Messali, B. Hammouti, A. Elidrissi, I. Warad, Der Pharma Chim. 3 (2011) 283.

[13] L. Chafki, E.H. Rifi, R. Touir, M.E. Touhami, and Z. Hatim, The Open Mater. Sci. J. 12 (2018) 68.

[14] M. Galai, H. Benqlilou, M.E. Touhami, T. Belhaj, K. Berrami, and H. El Kafssaoui, Environ. Eng. Res. 77 (2017) 164.

[15] H. Lgaz, R. Salghi, and H.I. Ali, Int. J. Electrochem. Sci. 13 (2018) 250.

[16] J. N. Asegbeloyin, P.M. Ejikeme, L.O. Olasunkanmi, A.S. Adekunle, E.E. Ebenso, Materials (2015) 2918.

[17] M. Ouakki, K. Dahmani, Z. Aribou, E. Ech-chihbi, M. Galai, N. AlZeqri, I. Warad, Z. Benzekri, L. Guo, A.A. AlObaid, O.H. Abd-Elkader, S. Boukhris, M. Cherkaoui, Inorganic Chem. Commun. 157 (2023) 111342.

[18] I. saber, Int. J. Electrochem. Sci. 19 (2024) 100815.

[19] F. Mansfeld, M.W. Kending, and S. Tsai, Corrosion 37 (1981) 301.

[20] K. Tebbji, B. Hammouti, H. Oudda, A. Ramdani, and M. Benkadour, Applied Surface (2005) 1378.

[21] M. Rbaa, M. Galai, Y. El Kacimi, M. Ouakki, R. Touir, and M.E. Touhami, Portugaliae Electrochim. Acta 35 (2017) 323.

[22] M. Galai, T. Anik, M.E. Touhami, E.H. Rifi, Z. Asfari, and R. Touir, Surface and Coatings Technol. 310 (2017) 16.

[23] A. Hamdouch, A. Anejjar, L. Bijla, S. Gharby, A. Asdadi, B. Chebli, R. Salghi, L.M.I. Hassani, Moroc. J. Chem. 11 (2023) 11.

[24] C. Merimi, B. Hammouti, K. Zaidi, B. Hafez, H. Elmsellem, R. Touzani, S. Kaya, J. Mol. Struct. 1278 (2023) 134883.

[25] O. Benali, L. Larabi, M. Traisnel, L. Gengenbre, and Y. Harek, Applied Surface Sci. 253 (2007) 6130.

[26] S. Jodeh, S. Al Masri, O. Hamed, M. Haddad, D. Jodeh, R. Salghi, S. Radi, J. Amarah, F. El-Hajjaji, and I. Warad, J. Mater. Environ. Sci. 7 (2016) 1037.

[27] X. Zheng, S. Zhang, W. Li, L. Yin, J. He, and J. Wua, Corr. Sci. 80 (2014) 383.

[28] M. Ouakki, M. Galai, Z. Benzekri, C. Verma, E. Ech-chihbi, S. Kaya, S. Boukhris, E.E. Ebenso, M.E. Touhami, and M. Cherkaoui, Colloids and Surfaces A: Physicochemical and Engineering Aspects 611 (2021**)** 125810.

[29] K. Dahmani, Z. Galai, M. Cherkaoui, A. El Hasnaoui, and A. El Hessni, JMES (2017**)** 1676.

[30] L. Afia, R. Salghi, A. Zarrouk, O. Benali, B. Hammouti, and L. Bazzi, Portugaliae Electrochim. Acta 30 (2012) 267.

[31] N. Errahmany, F. Hamouche, M. Nounah, I. Saber, S. Yaqouti, A. Nounah, A. Tazouti, R. Fakhreddine, R. Touir, H. El Kafssaoui, M. Chahboune. Moroccan Journal of Chemistry. 12 (2024) 1707.

[32] K. Dahmani, M. Khattabi, I. Saber, O. Kharbouch, M. Galai, S. M. Alharbi, F. Benhiba, A. Shaim, Z. S. Safi, M. Ebn Touhami, M. Cherkaoui. Chemistry Africa. 7 (2024) 5461.

[33] J. Marsh, Advanced Organic Chemistry, 3rd ed. Wiley Eastern, New Delhi (1988).

[34] M. Bouklah, O. Krim, M. Messali, B. Hammouti, A. Elidrissi, and I. Warad, Der Pharma Chim. (2011) 283.

[35] G. Avci, Mater. Chem. Phys. 112 (2008) 234.

[36] E. Bayol, A.A. Gurten, M. Dursun, and K. Kayakırılmaz, Acta Physico-Chimica Sinica 24 (2008) 2236.

[37] B. Zerga, A. Attayibat, M. Sfaira, M. Taleb, B. Hammouti, M. Ebn Touhami, S. Radi, Z. Rais. J. Appl. Electrochem. 40 (2010) 1575.
[38] A. K. Singh, and M. A. Quraishi, J. Appl. Chem. 40 (2010) 1293.
[39] M. Benabdellah, A. Aouniti, A. Dafali, B. Hammouti, M. Benkaddour, A. Yahyi, and A. Ettouhami, Appl. Surf. Sci. 252 (2006) 8341.
[40] N.C. Subramanyam, and S.M. Mayanna, Corros. Sci. 25 (1985) 163.
[41] N. Eldakar, and K. Nobe, Corrosion 36 (1981) 271.
[42] K. Kurosawa, and T. Fukushima, Corr. Sci. 29 (1989) 1103.
[43] Y.I. Kuznetsov, Prot. Met. 37 (2001) 101.
[44] Z. Aribou, M. Ouakki, N. Khemmou, S. Sibous, E. Ech-chihbi, Z. Benzekri, M. Galai, S. Boukhris, A.A. AlObaid, I. Warad, and M. EbnTouhami, J. Appl. Electrochem. 54 (2024) 393.
[45] A.A. Al-Amiery, L.M. Shaker, A.H. Kadhum, and M.S. Takriff, Mater. Today Proc. 42 (2021) 2968.
[46] R. Melian, M. Radi, M. Galai, M. Ouakki, E. Ech-chihbi, N. Dkhirche, L. Guo, M.E. Touhami, J. Mol. Liq. 331 (2021) 115661.
[47] G. Avci, Mater. Chem. Phys. 112 (2008) 234.
[48] M. Elayyachy, A. El Idrissi, and B. Hammouti, Corros. Sci. 48 (2006) 2470.
[49] E. Bayol, A.A. Gurten, M. Dursun, and K. Kayakırılmaz, Acta Phys. Chim. Sin. 24 (2008) 2236.
[50] A. Yurt, S. Ulutas, and H. Dal, Appl. Surf. Sci. 253 (2006) 919.
[51] M. Yadav, S. Kumar, N. Tiwari, I. Bahadur, and E.E. Ebenso, J. Mol. Liq. 212 (2015) 151.

Copyright © 2025 by CEE (Center of Excellence in Electrochemistry)

ANALYTICAL & BIOANALYTICAL ELECTROCHEMISTRY (http://www.abechem.com**)**

Reproduction is permitted for noncommercial purposes.